Dynamic Behaviour of Three-Dimensional Planetary Geared Rotor Systems

Ali Tatar [1*], Christoph W. Schwingshackl [1], Michael I. Friswell [2]

[1] Imperial College London, Department of Mechanical Engineering, London SW7 2AZ, United Kingdom

[2] Swansea University, College of Engineering, Swansea SA1 8EN, United Kingdom

* Corresponding author: a.tatar16@imperial.ac.uk
Tel: +44 777 806 9562

ABSTRACT

A six degrees of freedom dynamic model of a planetary geared rotor system with equally spaced planets is developed by considering gyroscopic effects. The dynamic model is created using a lumped parameter model of the planetary gearbox and a finite element model of the rotating shafts using Timoshenko beams. The gears and carrier in the planetary gearbox are assumed to be rigid, and the gear teeth contacts and bearing elements are assumed to be flexible. The modal analysis results show that torsional and axial vibrations on the shafts are coupled in the helical gearing configuration due to the gear helix angle whereas these vibrations become uncoupled for spur gearing. Mainly, the vibration modes are classified as coupled torsional-axial, lateral and gearbox for the helical gear configuration, and torsional, axial, lateral and gearbox for the spur gear configuration. Modal energy analysis is used to quantify the coupling level between the shafts and the planetary gearbox, highlighting the impact of the gearbox on certain mode families. Gyroscopic effects of the planetary gearbox are found to be of great importance in the gearbox dominated modes.

Keywords: Planetary gearbox; rotor dynamics; gear dynamics; geared rotor; modal analysis; modal energy

1. INTRODUCTION

Planetary gearboxes are widely used machine elements to transmit power and motion, and convert speed and torque in rotating systems since they provide compactness, higher gear ratio and power transmission capacity, and lower noise and vibration advantages [1,2]. Planetary geared systems can be seen in many engineering applications such as geared turbofan engines, automotive transmissions, wind turbines and 3D printers. Introducing a planetary gearbox into a rotating machine can directly affect its global dynamics due to the flexibility, damping and inertia of the planetary gearbox with gyroscopic effects, leading to a coupled dynamic response of the planetary gearbox and rotor. In addition, the planetary gearbox can become an excitation source in rotor systems because of the internal excitations caused by the time-varying mesh stiffness, profile modifications and manufacturing error, and the external excitations such as rotating mass imbalances and speed/torque fluctuations originating from the gears [3,4]. Due to the impact of a planetary gearbox on the dynamic response of the global system, the coupled dynamic behaviour of planetary geared rotor systems has recently become an important research topic.

A main focus of current research is the dynamic modelling and analysis of planetary gearboxes with different configurations such as single stage [5–8], two stages [9,10], multiple stages [11–16], compound [17–20] and double helical [21–25] sets. Two main dynamic modelling approaches, flexible and rigid body models, have been employed by researchers. In flexible body models, mostly ring gears [26–30] and planet carriers [26,27] are accepted as flexible elements. A fully coupled dynamic modelling method using virtual equivalent shaft elements has recently been proposed [15,16]. Flexible body models can be classified as two dimensional [28–30], including transverse (lateral) and rotational (torsional) degrees of freedom, and three dimensional [15,16,26,27] models. In rigid body models, the carrier and all gears (sun, planets, and ring) in the planetary gearbox are assumed to be rigid whereas the bearings and gear contacts are assumed to be flexible. Depending on the number of degrees of freedom, the rigid body dynamic models can be divided into three main groups: (i) purely torsional model, (ii) torsional - transverse model and (iii) three dimensional model [1]. The purely torsional model has one degree of freedom per node and can be used for the analyses of spur planetary gearboxes if transverse, tilting and axial motions, and gyroscopic effects are negligible [11,13,17,20,31,32]. Expanding the purely torsional model to include transverse motions leads to the three degrees of freedom per node torsional - transverse model [6,9,33,34]. This modelling approach can be employed for high speed applications of spur planetary gearboxes where gyroscopic effects can lead to motions in transverse directions [8]. Further modifications to the torsional - transverse model have led to the three dimensional model which includes six degrees of freedom per node (torsional, transverse, tilting, axial), and allows the capture of axial and tilting motions of planetary gearbox members [5,7,10]. This enables the analysis of helical planetary gear sets in which axial gear mesh forces can occur. Furthermore, dynamic models for double-helical planetary gear sets have been developed using the three dimensional model approach [22–25,33]. Dynamic analyses of three-dimensional models have also been conducted with gyroscopic effects [7,10,25]. Depending on the complexity of the model, different types of mode shapes can be obtained. The purely torsional model can only detect torsional modes, which can either be global modes, or planet modes [6,8,9,33]. The torsional - transverse model can provide rotational, translational and planet modes for the spur planetary gearbox whereas the most advanced three dimensional model approach leads to rotational-axial, translational-tilting and planet modes for the helical gearbox [7,23]. The sensitivity of modal parameters of the planetary gearbox (natural frequencies and mode shapes) with regards to the gearbox input parameters such as gear mesh and bearing stiffness, and gear mass, inertia and speed have also been analysed using these dynamic models [12,16,35,36]. To validate the modal behaviour of the dynamic models, some experimental studies were performed for spur planetary gear sets. Computed rotational, translational and planet modes in the torsional - transverse model were correlated with these experimental studies [34,37–39].

The coupled dynamic behaviour of geared rotor systems with gyroscopic effects has also been studied in great detail with a focus on the coupling effects of the gearbox due to its torsional, axial and lateral stiffness. Lateral-torsional coupling in spur geared rotors and lateral-torsional-axial coupling in helical geared rotors were shown by many studies [40–49]. Among these studies, the finite element method has become a popular tool for the dynamic analyses [41,42,44,45,48,49]. Although the dynamic behaviours of spur and helical geared rotor systems are well understood today, less research has been carried out to understand the dynamic behaviour of planetary geared rotor systems [50–57] . So far, one DOF torsional [50–52], five DOF lateral-torsional [53] and six DOF lateral-torsional-axial [54–57] models of planetary geared rotor systems have been investigated for wind turbine and geared turbofan engine applications. From this research, only two of the six DOF models have taken gyroscopic effects into account for geared turbofan engine applications [56,57]. Wei et al. [57] considered the forced vibration analysis of a geared turbofan engine due to loss of a blade creating rotating imbalance. Tatar and Schwingshackl [56] used a low fidelity model of the planetary gearbox, including uncoupled gearbox stiffness, to investigate the planetary gearbox impact on the dynamics of the rotor system. The modal behaviour of planetary geared rotor systems is still only partially understood, and more work is needed to provide a full understanding of the dynamic behaviour of such systems.

To provide further insight into the dynamic behaviour of planetary geared rotor systems, a six degrees of freedom dynamic model is presented in this paper. For this purpose, a three-dimensional model of an equally spaced planetary gearbox and a rotor system are created by employing the lumped parameter and finite element methods respectively. 1-D rotating Timoshenko beam elements for the shafts and uncoupled linear spring elements for the bearings are used to construct the dynamic model of the rotor system. The planetary gearbox is introduced to couple the two shafts together. Gyroscopic effects of the shafts and planetary gearbox are included in the analysis. The modal behaviour of the global rotor system is identified based on the mode shapes of the shafts. The impact of the planetary gearbox on the dynamic behaviour of the rotating system is analysed by modal energy analysis.

2. DYNAMIC MODEL OF A PLANETARY GEARED ROTOR SYSTEM

A basic planetary geared rotor system consists of two shafts, several bearings and a planetary gearbox. Figure 1 shows such a basic system where the two shafts rotate at different speeds. The shafts are coupled by the planetary gearbox and supported via the bearing elements at each end. The planetary gearbox is also grounded via its bearings.

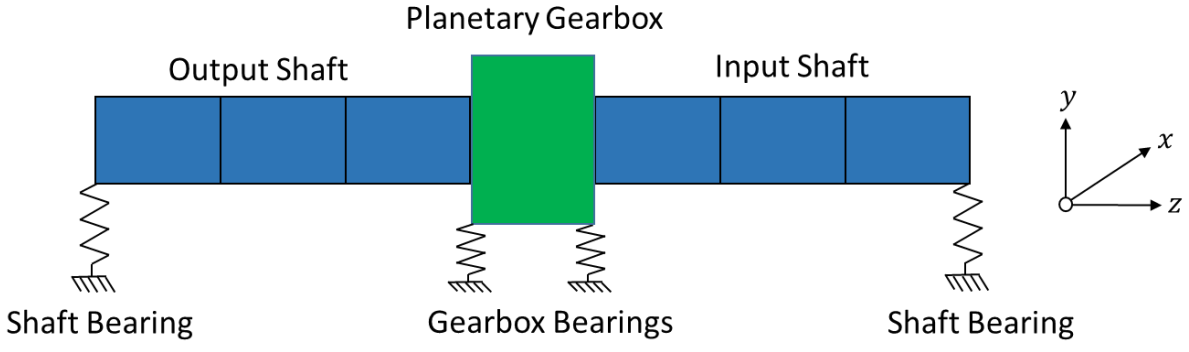

Figure 1: Planetary geared rotor system

In this section, some background on the rotor and planetary gearbox modelling will be provided, before the planetary geared rotor model for the system in Figure 1 is created. Throughout the work, the stationary coordinate system is employed for the dynamic model and the generalized coordinates are written as

$$\boldsymbol{q} = [x, y, z, \theta_x, \theta_y, \theta_z]. \tag{1}$$

where the generalized coordinates include transverse(x, y), axial(z), tilting (θ_x, θ_y) and torsional (θ_z) motions.

2.1. Shafts

Longer rotating shafts can be modelled as flexible beams where their mass, stiffness and gyroscopic matrices can be obtained using the finite element method [58]. Due to the high number of modes included in this study, Timoshenko beam elements are used to capture potential shear deflection and rotational inertia terms [58]. Each beam element has two nodes with twelve degrees of freedom, including transverse, tilting, axial and torsional directions. The geometry of the beam element with its local coordinates can be seen in Figure 2.

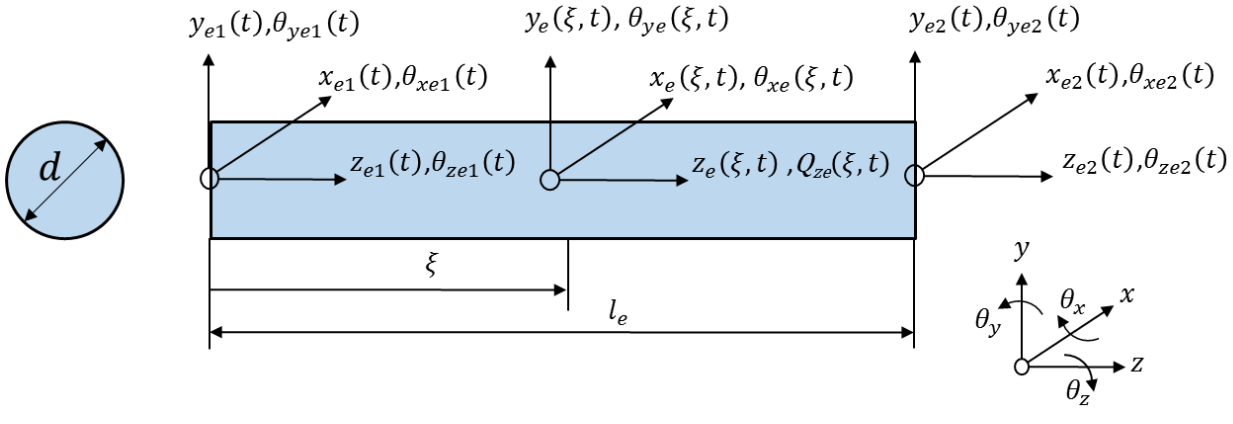

Figure 2: The shaft finite element

The local coordinates, $\boldsymbol{q}_e(t)$, and shape functions, $\boldsymbol{N}_e(\xi)$, for this beam element can be expressed as [58]

$$\begin{aligned}\boldsymbol{q}_e(t) &= \left[x_{e1}(t), y_{e1}(t), z_{e1}(t), \theta_{xe1}(t), \theta_{ye1}(t), \theta_{ze1}(t), x_{e2}(t), y_{e2}(t), z_{e2}(t), \theta_{xe2}(t), \theta_{ye2}(t), \theta_{ze2}(t)\right] \\ \boldsymbol{N}_e(\xi) &= [N_{e1}(\xi), N_{e2}(\xi), N_{e3}(\xi), N_{e4}(\xi), N_{e5}(\xi), N_{e6}(\xi), N_{e7}(\xi), N_{e8}(\xi), N_{e9}(\xi), N_{e10}(\xi), N_{e11}(\xi), N_{e12}(\xi)]\end{aligned} \tag{2}$$

The deflections, $\boldsymbol{q}_e(\xi, t)$, throughout the beam element can then be approximated by multiplying the shape functions and local coordinates with the Hadamard product as

$$\begin{aligned}\boldsymbol{q}_e(\xi, t) &= \boldsymbol{N}_e(\xi) \circ \boldsymbol{q}_e(t), \\ \boldsymbol{q}_e(\xi, t) &= [x_{e1}(\xi, t), y_{e1}(\xi, t), z_{e1}(\xi, t), \theta_{xe1}(\xi, t), \theta_{ye1}(\xi, t), \theta_{ze1}(\xi, t), \\ &\quad x_{e2}(\xi, t), y_{e2}(\xi, t), z_{e2}(\xi, t), \theta_{xe2}(\xi, t), \theta_{ye2}(\xi, t), \theta_{ze2}(\xi, t)].\end{aligned} \tag{3}$$

Then, the kinetic, T_s, and potential, V_s, energies of an individual Timoshenko beam element become [42,48,58,59]

$$\begin{aligned}T_s &= \frac{1}{2}\int_0^{l_e} \rho_e \left\{A_e\left(\dot{x}_e{}^2 + \dot{y}_e{}^2 + \dot{z}_e{}^2\right) + I_e\left(\dot{\theta}_{xe}{}^2 + \dot{\theta}_{ye}{}^2\right) + J_e\left[\left(\Omega_e + \dot{\theta}_{ze}\right)^2 + \left(\Omega_e + \dot{\theta}_{ze}\right)\left(\theta_{ye}\dot{\theta}_{xe} - \theta_{xe}\dot{\theta}_{ye}\right)\right]\right\} d\xi, \\ V_s &= \frac{1}{2}\int_0^{l_e} \left\{E_e I_e\left(\theta_{xe}'{}^2 + \theta_{ye}'{}^2\right) + G_e J_e\left(\theta_{ze}'\right)^2 + \kappa_e G_e A_e\left[\left(x_e' - \theta_{ye}\right)^2 + \left(y_e' + \theta_{xe}\right)^2\right] + E_e A_e\left(z_e'\right)^2\right\} d\xi.\end{aligned} \tag{4}$$

where the dot $\dot{}$ and prime $'$ denote differentiation with respect to time and ξ respectively. The kinetic energy includes the transverse, axial, tilting and torsional motions with gyroscopic terms. The potential energy includes axial, torsional, bending and shear deflections where the shear constant, κ_e, for a solid shaft is [58]

$$\kappa_e = \frac{6(1+\nu_e)}{(7+6\nu_e)}. \tag{5}$$

Following the energy equations, the finite element formulations for the mass, gyroscopic and stiffness element matrices are obtained by applying the Lagrange`s equations of the second kind. The full mathematical derivation of the mass, stiffness, gyroscopic matrices and shape functions of the system can be found in reference [58], and the 12 DOF finite element matrices are given explicitly in reference [48]. Damping can also be added to the shaft model via proportional damping [60] as

$$\mathbf{C}_s = \alpha_1 \mathbf{M}_s + \alpha_2 \mathbf{K}_s. \tag{6}$$

Finally, the mass, $\mathbf{M}_s$, stiffness, $\mathbf{K}_s$, damping, $\mathbf{C}_s$, gyroscopic, $\mathbf{G}_s$ matrices of the shafts are obtained using the element matrices.

2.2. Bearings

Bearings are used to support the rotating systems, which can be either rigid or flexible, depending on the application. A range of bearing element models is available in the literature, ranging from simple linear models to advanced nonlinear dynamic models [58]. In the present model, the bearing elements are assumed to be flexible and consist of linear translational and rotational spring elements. The stiffness, $\mathbf{K}_b$, and damping, $\mathbf{C}_b$, matrices of the bearing elements are written as [58]

$$\begin{aligned}\mathbf{K}_b &= \mathrm{diag}\left(k_x, k_y, k_z, k_{Q_x}, k_{Q_y}, k_{Q_z}\right), \\ \mathbf{C}_b &= \mathrm{diag}(c_x, c_y, c_z, c_{Q_x}, c_{Q_y}, c_{Q_z}).\end{aligned} \tag{7}$$

As seen in Eq. (7), the matrices are in diagonal form which means that the bearings consist of uncoupled stiffness and damping elements. Torsional stiffness, k_{Q_z}, and damping, c_{Q_z}, of the bearing elements will be assumed to be zero, allowing the shaft to rotate freely without any resistance. This study focuses on the understanding of the impact of a planetary gearbox on the dynamics of the rotor system and for that reason basic bearing elements with no coupling terms are considered sufficient for this study.

2.3. Planetary Gearbox

A basic single stage planetary gearbox consists of a ring gear, a carrier, a sun gear and *N* planet gears. A six degrees of freedom linear lumped parameter of a planetary gearbox is employed for the dynamic modelling from references [5,21,22]. In this model, all the members of the planetary gearbox, which are the sun, ring and planet gears and the carrier, are assumed to be

rigid disks. The gear teeth contacts and bearing elements are assumed to be flexible. Linear time varying mesh stiffness and clearance nonlinearity due to loss of teeth contact are neglected. All the planet gears have the same property and they are equally spaced. As seen schematically in Figure 3, the gear teeth contacts are represented with linear springs, which are between the sun and planet gears (k_{sp}), and between the planet gears and the ring gear (k_{rp}). These gear teeth contacts are also known as gear mesh stiffness, which are assumed to be constant in the model due to the linear spring elements [5,21,22]. All the planetary gearbox members have six DOF bearing elements, represented by linear springs (k_r, k_c, k_s, k_p) defined in Eq. (7).

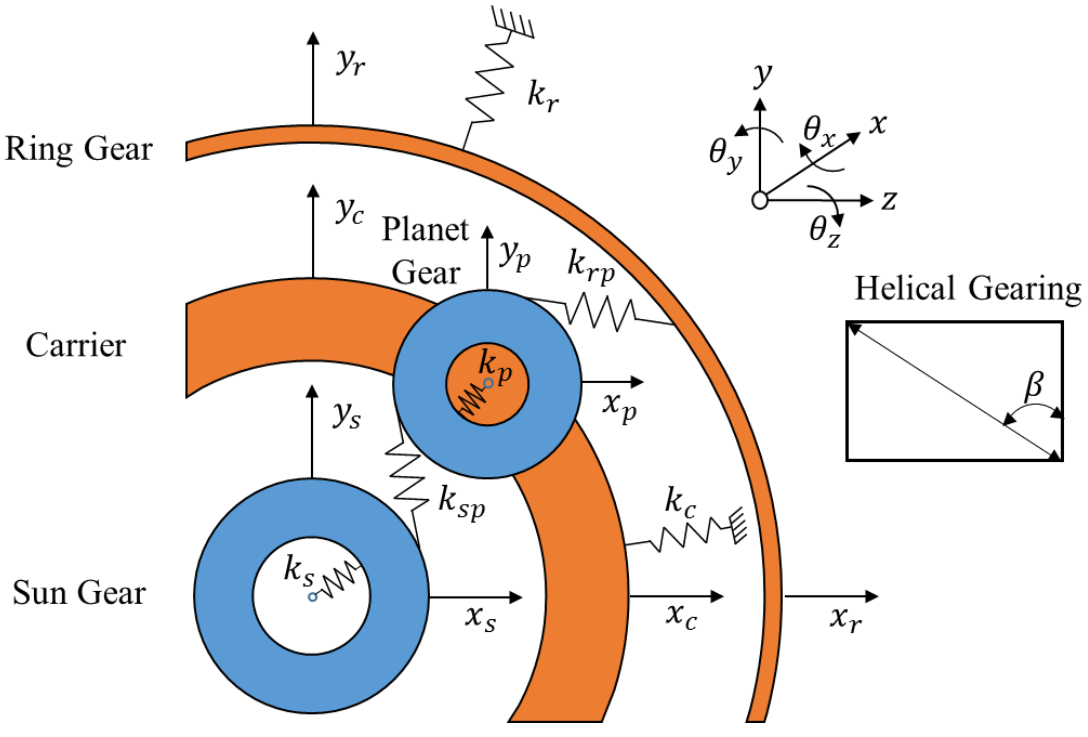

Figure 3: Dynamic model of a planetary gearbox

The equation of motion of the planetary gearbox is obtained using Lagrange's equations. For this purpose, the total kinetic and potential energies of the system must be obtained. With the small rotation assumption in the θ_{xh} and θ_{yh} tilting directions, the kinetic energies of the central members (ring gear, sun gear and carrier) and planet gears can be written as

$$T_h = \frac{1}{2}\sum_{h=1}^{3} m_h\left(\dot{x}_h{}^2 + \dot{y}_h{}^2 + \dot{z}_h{}^2\right) + I_{dh}\left(\dot{\theta}_{xh}{}^2 + \dot{\theta}_{yh}{}^2\right) + I_{ph}\left(\Omega_h{}^2 - 2\Omega_h\dot{\theta}_{yh}\theta_{xh} + \dot{\theta}_{zh}{}^2\right)$$
$$T_p = \frac{1}{2}\sum_{i=1}^{N} m_{pi}\left(\dot{x}_{pi}{}^2 + \dot{y}_{pi}{}^2 + \dot{z}_{pi}{}^2\right) + I_{dpi}\left(\dot{\theta}_{xpi}{}^2 + \dot{\theta}_{ypi}{}^2\right) + I_{ppi}\left(\Omega_{\mathrm{pi}}{}^2 - 2\Omega_{pi}\dot{\theta}_{ypi}\theta_{xpi} + \dot{\theta}_{zpi}{}^2\right) \quad (8)$$

respectively [58]. Here, h is the central member index for the ring gear, carrier and sun. The kinetic energies include all motions in three dimensions with gyroscopic terms, similar to the kinetic energy of the Timoshenko beam elements, defined in Eq. (4). The gyroscopic terms in the gearbox originate from the $\dot{\theta}_y\theta_x$ multiplication. The strain energies of the bearings for the central members and planet gears can be written respectively as [21]

$$V_h = \frac{1}{2}\sum_{h=1}^{3} k_{xh}x_h{}^2 + k_{yh}y_h{}^2 + k_{zh}z_h{}^2 + k_{\theta_{xh}}\theta_{xh}{}^2 + k_{\theta_{yh}}\theta_{yh}{}^2 + k_{\theta_{zh}}\theta_{zh}{}^2$$
$$V_p = \frac{1}{2}\sum_{i=1}^{N} k_{xp}\left(x_c - x_{pi} - r_c\theta_{zc}\sin\alpha_{pi}\right)^2 + k_{yp}\left(y_c - y_{pi} + r_c\theta_{zc}\cos\alpha_{pi}\right)^2 \quad (9)$$
$$+ k_{zp}\left(z_c - z_{pi} + r_c\theta_{xc}\sin\alpha_{pi} - r_c\theta_{yc}\cos\alpha_{pi}\right)^2 + k_{\theta_{xp}}\left(\theta_{xc} - \theta_{xpi}\right)^2 + k_{\theta_{yp}}\left(\theta_{yc} - \theta_{ypi}\right)^2$$

where α_{pi} is the angular position of each planet, which can be defined for the non – rotating carrier configuration as

$$\alpha_{pi+1} = \alpha_{pi} + \frac{2\pi}{N}. \quad (10)$$

Here, α_{p1} represents the first planet`s angular position, which is assumed to be zero. The torsional stiffnesses of the rotating members in the planetary gearbox are assumed to be zero based on the planetary gearbox configurations. For instance, torsional bearing stiffnesses of the ring, sun and planet gears are set as zero in the rotating ring – fixed carrier configuration since the gears rotate and the carrier does not rotate in this configuration. Another potential energy component given by the gear mesh strain energy due to gear teeth deflections must also be included in the model [21] as

$$V_m = \sum_{i=1}^{N} \frac{1}{2} k_{sp} {\delta_{spi}}^2 + \frac{1}{2} k_{rp} {\delta_{rpi}}^2 \tag{11}$$

where δ_{spi} and δ_{rpi} represent the relative displacement between the sun-planet and ring-planet gear meshes respectively. These relative displacements depend on the geometry of the gear meshes and can be expressed as

$$\begin{aligned} \delta_{spi} &= \left[\left(x_s - x_{pi}\right)\sin\psi_{spi} + \left(y_s - y_{pi}\right)\cos\psi_{spi} + \left(r_s\theta_{zs} + r_p\theta_{zpi}\right)\right]\cos\beta \\ &+ \left[\left(r_s\theta_{xs} + r_p\theta_{xpi}\right)\sin\psi_{spi} + \left(r_s\theta_{ys} + r_p\theta_{ypi}\right)\cos\psi_{spi} + \left(z_{pi} - z_s\right)\right]\sin\beta \\ \delta_{rpi} &= \left[\left(x_{pi} - x_r\right)\sin\psi_{rpi} + \left(y_r - y_{pi}\right)\cos\psi_{rpi} + \left(r_r\theta_{zr} - r_p\theta_{zpi}\right)\right]\cos\beta \\ &+ \left[\left(r_r\theta_{xr} - r_p\theta_{xpi}\right)\sin\psi_{rpi} + \left(r_p\theta_{ypi} - r_r\theta_{yr}\right)\cos\psi_{rpi} + \left(z_r - z_{pi}\right)\right]\sin\beta \end{aligned} \tag{12}$$

where β is the gear helix angle. A spur gear configuration for the planetary gearbox can be obtained by setting the helix angle, β, to zero. In Eq. (12), ψ is the angle between the plane of action and the vertical *y* axis, which is defined for a counter clockwise motion of the sun gear as [21,22]

$$\begin{aligned} \psi_{spi} &= \phi_{sp} - \alpha_{pi} \\ \psi_{rpi} &= \phi_{rp} + \alpha_{pi} \end{aligned} \tag{13}$$

for the sun-planet and ring-planet gear meshes respectively. Here, ϕ_{sp} and ϕ_{rp} are the transverse pressure angles of the sun-planet and the ring-planet gear meshes respectively [21,22]. The total kinetic and potential energies of the planetary gearbox can then be computed as

$$\begin{aligned} T &= T_h + T_p, \\ V &= V_h + V_p + V_m. \end{aligned} \tag{14}$$

Finally, the planetary gearbox equation of motion can be derived using Lagrange's second equation as

$$\mathbf{M_g}\ddot{\boldsymbol{q}}_{\boldsymbol{g}}(t) + \left[\mathbf{C}_g + \mathbf{G}_g\left(\Omega_h, \Omega_{\mathrm{pi}}\right)\right]\dot{\boldsymbol{q}}_{\boldsymbol{g}}(t) + \mathbf{K}_g\boldsymbol{q}_{\boldsymbol{g}}(t) = 0 \tag{15}$$

which leads to the mass, $\mathbf{M_g}$, stiffness, $\mathbf{K}_g$, gyroscopic $\mathbf{G}_g$ matrices of the planetary gearbox. Proportional damping defined in Eq. (5) may also be employed for the damping of the planetary gearbox, $\mathbf{C}_g$. It must be noted that $\boldsymbol{q}_g(t)$ in Eq. (15) represents the generalized coordinates for the gearbox. The full mass, stiffness and gyroscopic matrices can be seen in references [5,21,22].

2.4. Assembly of the Planetary Geared Rotor System

The general equation of motion of a planetary geared rotor system with *n* degrees of freedom system can be obtained after the assembly of the shafts, bearings and planetary gearbox matrices. The global mass, **M**, gyroscopic, **G**, stiffness, **K**, and damping matrices, **C**, are obtained using the standard assembly methods for FE analysis and defined as

$$\begin{aligned} [\mathbf{M}] &= \mathbf{M}\left(\mathbf{M_s}, \mathbf{M_g}\right), \\ [\mathbf{G}] &= \mathbf{G}\left(\mathbf{G_s}, \mathbf{G_g}\right), \\ [\mathbf{K}] &= \mathbf{K}\left(\mathbf{K_s}, \mathbf{K_b}, \mathbf{K_g}\right), \\ [\mathbf{C}] &= \mathbf{C}\left(\mathbf{C_s}, \mathbf{C_b}, \mathbf{C_g}\right). \end{aligned} \tag{16}$$

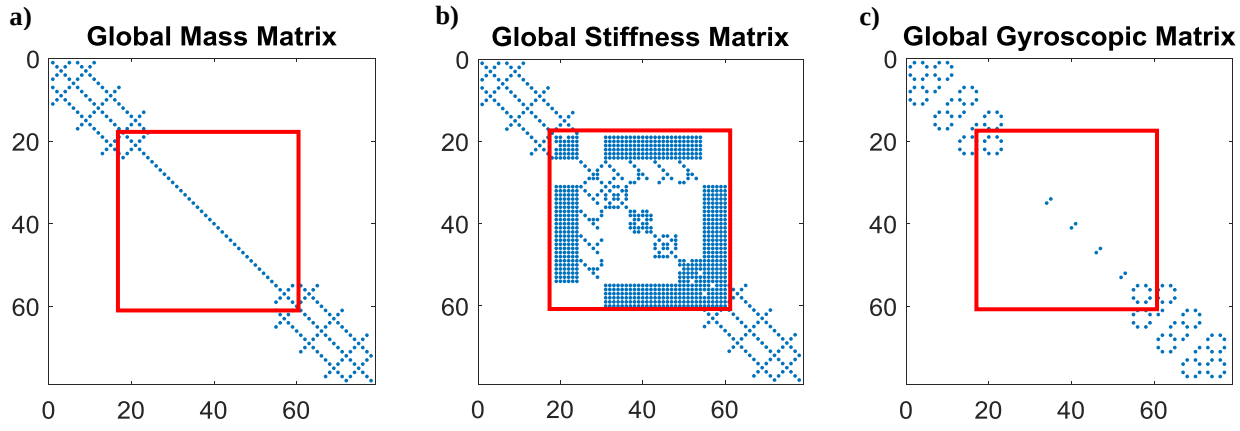

Figure 4: Global matrices with 78 DOFs, a) mass, b) stiffness, c) gyroscopic.

Figure 4 shows the general distribution of entries in the global matrices where mass and stiffness matrices are symmetric while the gyroscopic matrix is skew-symmetric. The planetary gearbox contribution in the matrices is highlighted by the red frames where the mass matrix of the planetary gearbox is in diagonal form and the gyroscopic matrix of the planetary gearbox is skew-symmetric. The stiffness matrix of the planetary gearbox makes the dynamic problem coupled since coupling terms arise. Finally, the system equation of the planetary geared rotor system for free responses can be written as

$$\mathbf{M}\ddot{\boldsymbol{q}}(t) + \left[\mathbf{C} + \mathbf{G}\left(\Omega_h, \Omega_{\mathrm{pi}}\right)\right]\dot{\boldsymbol{q}}(t) + \mathbf{K}\boldsymbol{q}(t) = 0. \tag{17}$$

In this model, the input and output shafts are rigidly connected to the input and output members of the planetary gearbox. For the rotating ring-fixed carrier gear configuration, the input and output members of the planetary gearbox thereby become the sun and ring gears respectively. In the case of the rotating carrier-fixed ring configuration the carrier becomes the output member whilst the sun gear remains the input member. Speed ratios of the planetary gearbox members can be obtained for the different configurations from the reference [61]. The model presented in this paper allows to analyse a rotating ring – fixed carrier configuration of the planetary gearbox, but is not sufficient to analyse a configuration with a rotating carrier since the spacing angles are currently constant, and the centripetal acceleration of the planets is not included in the formulation.

3. MODAL ANALYSIS

3.1. Eigenvalue Problem of Rotating Systems

The natural frequencies and mode shapes of the previously introduced system can be obtained from a free-free modal analysis by solving the eigenvalue problem. As can be seen from Eq. (17), gyroscopic and damping matrices make the eigenvalue problem of rotating systems quadratic, and therefore the state-space form is used to reduce the order of the eigenvalue problem from two to one. To construct the state-space representation, the system equation of motion (Eq. (17)) is reformulated as [62,63]

$$\ddot{\boldsymbol{q}}(t) + \mathbf{M}^{-1}\left[\mathbf{C} + \mathbf{G}\left(\Omega_h, \Omega_{\mathrm{pi}}\right)\right]\dot{\boldsymbol{q}}(t) + \left(\mathbf{M}^{-1}\mathbf{K}\right)\boldsymbol{q}(t) = 0. \tag{18}$$

Then, the standard eigenvalue problem in state – space form becomes

$$\begin{Bmatrix}\dot{\boldsymbol{q}}\\ \ddot{\boldsymbol{q}}\end{Bmatrix} = \begin{bmatrix}\mathbf{0} & \boldsymbol{I}\\ -\mathbf{M}^{-1}\mathbf{K} & -\mathbf{M}^{-1}\left[\mathbf{C} + \mathbf{G}\left(\Omega_h, \Omega_{\mathrm{pi}}\right)\right]\end{bmatrix}\begin{Bmatrix}\boldsymbol{q}\\ \dot{\boldsymbol{q}}\end{Bmatrix} \tag{19}$$

where $\begin{Bmatrix}\boldsymbol{q}\\ \dot{\boldsymbol{q}}\end{Bmatrix}$ and $\begin{Bmatrix}\dot{\boldsymbol{q}}\\ \ddot{\boldsymbol{q}}\end{Bmatrix}$ are the state vectors, $\boldsymbol{x}$ and $\dot{\boldsymbol{x}}$ respectively. The standard eigenvalue problem can then be rewritten as

$$\{\dot{\boldsymbol{x}}\}_{2n\times 1} = [\mathbf{A}]_{2n\times 2n}\{\boldsymbol{x}\}_{2n\times 1}. \tag{20}$$

Although the eigenvalue problem is now first order, the size of the eigenvalue problem has doubled, and as a result doubling the size of the eigenvalue and eigenvector matrices. After solving the standard eigenvalue problem, the eigenvalue and eigenvector matrices are written as

$$\begin{matrix}[\lambda]_{2n\times 2n}\\ [\phi]_{2n\times 2n}\end{matrix} \tag{21}$$

respectively. It should be noted that these matrices consist of complex conjugate pairs. Finally, the mode shapes are extracted from the eigenvector matrix $[\phi]$ and the natural frequencies are obtained using the eigenvalues $[\lambda]$ as [63]

$$\omega_i = \sqrt{Re(\lambda_i)^2 + Im(\lambda_i)^2} \tag{22}$$

In this analysis, the standard eigenvalue solution is used rather than the generalized one to compute the eigenvalues and eigenvectors because of its higher accuracy and computational performance [62,63].

3.2. Mode Identification

Mode shapes in rotor systems can either be uncoupled with no interaction between the lateral, axial and torsional vibration of the system, or coupled where these modes can interact. A simple cyclically symmetric rotor system can be considered as uncoupled [58], but the presence of a gearbox in the system can lead to lateral, torsional and axial mode interaction [42,45–47,49]. To quantify the impact of a planetary gearbox on the coupling behaviour of the global modes of the geared rotor system, a modal energy approach is used where the modal energy of the gearbox for each mode is compared to the total modal energy in the system. The total modal energies of the rotor system and the planetary gearbox are computed by summing their kinetic and potential energies. The kinetic, T_r, potential, V_r, and total, L_r, energies of the rotor system are written as

$$\begin{aligned} T_r(i) &= \frac{1}{2}[\dot{\boldsymbol{q}}_r(i)]^T[\mathbf{M}][\dot{\boldsymbol{q}}_r(i)], \\ V_r(i) &= \frac{1}{2}[\boldsymbol{q}_r(i)]^T[\mathbf{K}][\boldsymbol{q}_r(i)], \\ L_r(i) &= T_r(i) + V_r(i). \end{aligned} \tag{23}$$

Similarly, the kinetic, potential and total energies of the planetary gearbox in the rotor system can be written respectively as

$$\begin{aligned} T_r^g(i) &= \frac{1}{2}[\dot{\boldsymbol{q}}_r(i)]^T\left[\mathbf{M}_g\right][\dot{\boldsymbol{q}}_r(i)], \\ V_r^g(i) &= \frac{1}{2}[\boldsymbol{q}_r(i)]^T\left[\mathbf{K}_g\right][\boldsymbol{q}_r(i)], \\ L_r^g(i) &= T_r^g(i) + V_r^g(i). \end{aligned} \tag{24}$$

In Eqs. (23) and (24), $\boldsymbol{q}_r$ is the motion vector in translational and rotational directions for each mode, defined as

$$\boldsymbol{q}_r = [q_{r1}, q_{r2}, q_{r3}, q_{r4}, q_{r5}, q_{r6}, \dots\dots\dots\dots\dots\dots\dots\dots\dots\dots, q_{rk}]. \tag{25}$$

where k represents the number of degrees of freedom of the system and r is the mode number. q_{rk} is defined as a function a of time as [64]

$$q_{rk}(i) = \phi_{rk} \sin\left(\frac{2\pi t(i)}{T_r} + \varphi_{rk}\right) \tag{26}$$

where $t(i)$ is the discrete time for the simulation. ϕ_{rk} and φ_{rk} represent the individual elements of the r^{th} eigenvector and its corresponding phase angle respectively. In Eq. (25), T_r is the vibration period of the r^{th} mode [64]. The discrete time is also defined as

$$t(i) = [0{:}\,\Delta t{:}\,t_s] \tag{27}$$

where Δt is time step, i is the index for the number of time data points and t_s is the vibration simulation time. By using the total energies from Eqs. (23) and (24), the mean values of the total energies of the global rotor system and the gearbox can be computed as

$$\begin{aligned} L_r &= \frac{1}{n}\sum_{i=1}^{n} L_r(i), \\ L_r^g &= \frac{1}{n}\sum_{i=1}^{n} L_r^g(i). \end{aligned} \tag{28}$$

The modal energy percentage of the gearbox then becomes

$$\varepsilon = \frac{L_r^g}{L_r} \times 100 \tag{29}$$

which allows an estimate of the gearbox contribution to the overall dynamic response of the system. It should be noted that damping will be neglected in the following numerical analysis, since it does not affect the presented results significantly and the modal energy defined in Eq. (29) can be computed for undamped cases.

Table 1: Parameters of the planetary geared rotor system

Parameter	Output Shaft	Input Shaft	Carrier	Ring	Planets	Sun
Length [m]	2	2	0.02	0.1	0.1	0.1
Outer Diameter [m]	0.2	0.2	0.63	0.7	0.2	0.23
Inner Diameter [m]			0.23	0.63	0.18	0.2
Material density [kg/m^3]	7800	7800	7800	7800	7800	7800
Young`s modulus [GPa]	211	211				
Shear modulus [GPa]	81.2	81.2				
Proportional damping α_1 constant	0	0	0	0	0	0
Proportional damping α_2 constant	0	0	0	0	0	0
Bearing radial stiffness [N/m]	10^9	10^9	10^9	10^9	10^9	10^9
Bearing axial stiffness [N/m]	10^9	10^9	10^9	10^9	10^9	10^9
Bearing tilting stiffness [N.m/rad]	10^7	10^7	10^7	10^7	10^7	10^7
Bearing torsional stiffness [N.m/rad]	0	0	10^{11}	0	0	0
Bearing radial damping [N/(m/s)]	0	0	0	0	0	0
Bearing axial damping [N/(m/s)]	0	0	0	0	0	0
Bearing tilting damping [N.m/(rad/s)]	0	0	0	0	0	0
Bearing torsional damping [N.m/(rad/s)]	0	0	0	0	0	0
Helix angle β [deg]				30	30	30
Transverse pressure angle ϕ [deg]				22.5	22.5	22.5
Mesh Stiffness [N/m]				10^8	10^8	10^8
Number of planets					4	
Number of beam elements	18	18				

3.2.1 Helical Planetary Geared Rotor

Modal analysis of the helical planetary gearbox on its own, and also the corresponding geared rotor system were conducted. Initially, an undamped non-rotating (static) case with the model parameters given in Table 1 was considered. The shafts from Figure 1 were modelled with 36 finite Timoshenko beam elements, and the planetary gearbox was modelled with seven rigid masses which represent the ring, carrier, sun and four planet gears. Modal analysis results are given for the first thirty modes in Table 2 where natural frequencies and mode types of the planetary gearbox and the planetary geared rotor system are listed. It should be noted that the first mode of the planetary geared rotor and the gearbox on its own are rotational rigid body modes due to the free rotation of the shafts and gears in rotational θ_Z direction. In addition, the modal energy percentage of the planetary gearbox for each global mode was also computed using Eq. (29), and is shown in Table 2.

Three main mode families can be identified from the modal analysis of the helical planetary gearbox, consisting of (i) rotational-axial, (ii) translational-tilting and (iii) planet modes. This definition is in accordance with Eritenel and Parker [7], where for the planet modes, the central members (ring, carrier and sun) do not move in any direction while the planets can freely move in all directions. In the case of the rotational-axial mode, the central members only move in rotational and axial directions while the planets move in all directions. Likewise, if the mode is translational-tilting, the central members only move in the translational and tilting directions, and the planets move in all directions. These coupling effects in the gearbox will have a significant impact on the geared rotor system, since it can lead to coupling terms in the equation of motion, and consequently lead to coupling between the two rotors that are connected via the gearbox. It is worth stating that this mode identification is valid for applications with more than one planet because one planet leads to coupled translational-tilting-rotational-axial modes.

As listed in Table 2, the mode shapes of the helical planetary geared rotor systems can be classified as (i) torsional-axial, (ii) lateral (bending) and (iii) gearbox modes. Figure 5 shows the first nine mode shapes of the rotor system. As stated, the first mode is a pure torsional rigid body mode, where the two shafts rotate around their axes as rigid bodies, and the gearbox determines the speed ratio. The following lateral modes of the shafts come in orthogonal pairs, and they are coupled due to the translational and tilting motion of the gearbox. Due to the helical configuration of the gearbox, an axial motion of the rotor can lead to a torsional motion and vice versa, which in turn leads to a torsional-axial mode coupling, as can be seen in Figure 5 for modes 6, 7 and 8. In the coupled torsional-axial modes, mode shape decoupling in the axial direction can also be seen between the two shafts due to the relatively high shaft stiffness compared to the gearbox. The final set of observed modes shapes for the geared rotor system are the isolated gearbox modes, which are associated with the planet modes of the gearbox itself. As previously discussed for the gearbox planet modes, the central members do not move, and consequently no vibration transmission from the planets to the shafts can occur. Since these modes are independent from the rotor system, the resonance frequencies are identical to the gearbox only computation.

Table 2: Modes of the helical planetary geared rotor and just the gearbox

	Helical Planetary Geared Rotor			Helical Planetary Gearbox	
Mode #	Gearbox Modal Energy %	Natural Frequency [Hz]	Mode Type	Natural Frequency [Hz]	Mode Type
1	27	0	Torsional (Rigid Body)	0	Rotational (Rigid Body)
2	10	114	Lateral	299	Translational - Tilting
3	10	114	Lateral	299	Translational - Tilting
4	10	115	Lateral	324	Translational - Tilting
5	10	115	Lateral	324	Translational - Tilting
6	60	220	Torsional - Axial	524	Rotational - Axial
7	29	301	Torsional - Axial	633	Rotational - Axial
8	27	318	Torsional - Axial	642	Translational - Tilting
9	94	322	Lateral	642	Translational - Tilting
10	94	322	Lateral	711	Translational - Tilting
11	17	333	Lateral	711	Translational - Tilting
12	17	333	Lateral	735	Rotational - Axial
13	15	346	Lateral	908	Planet
14	15	346	Lateral	1018	Translational - Tilting
15	20	466	Torsional - Axial	1018	Translational - Tilting
16	62	508	Lateral	1227	Rotational - Axial
17	62	508	Lateral	1895	Translational - Tilting
18	97	595	Torsional - Axial	1895	Translational - Tilting
19	23	601	Lateral	1905	Rotational - Axial
20	23	601	Lateral	2263	Translational - Tilting
21	32	649	Lateral	2263	Translational - Tilting
22	32	649	Lateral	2332	Planet
23	84	710	Lateral	2367	Rotational - Axial
24	84	710	Lateral	2428	Planet
25	18	782	Torsional - Axial	2437	Translational - Tilting
26	28	873	Lateral	2437	Translational - Tilting
27	28	873	Lateral	2464	Planet
28	100	908	Gearbox	2484	Rotational - Axial
29	18	943	Lateral	2869	Translational - Tilting
30	18	943	Lateral	2869	Translational - Tilting

Figure 5 also shows that there is an asymmetric motion in the two shafts despite the fact that the planetary gearbox is located between the identical two shafts. This phenomenon occurs due the different mass and inertia properties of the input and output members of the planetary gearbox itself.

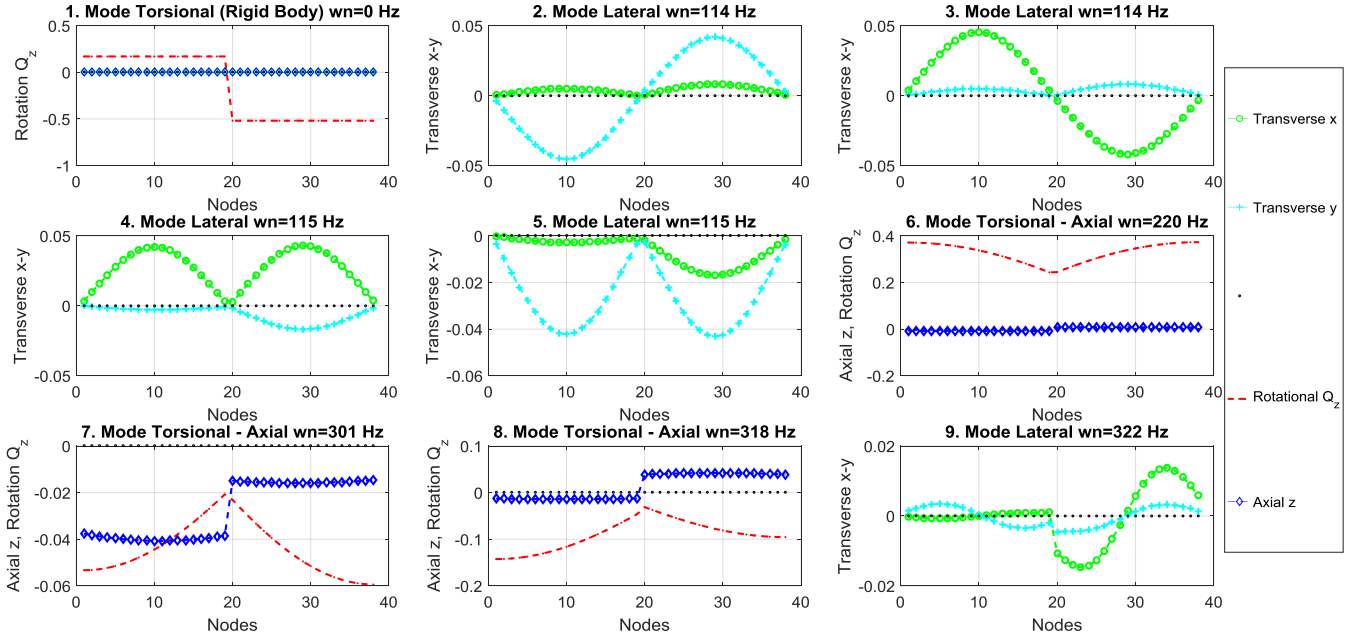

Figure 5: Mode shapes of the helical planetary geared rotor system

In order to better understand the gearbox contribution to the overall mode shape of the rotor system, the gearbox modal energy values from Table 2 can be considered. The planetary gearbox modal energy of the global system is 100% for each gearbox mode. These modes coincide with the planet modes of the gearbox itself. For example, the 13th mode of the planetary gearbox is a planet mode at 908 Hz, and also seen as the 28th mode of the planetary geared rotor system as a gearbox mode. There is no deflection on the shaft in any direction for these particular gearbox modes. There are also some other global modes in which gearbox has higher modal energies. For instance, the gearbox has higher modal energies for the 9th, 10th, 18th, 23rd and 24th global modes where the modal energy percentages are 94%, 94%, 97%, 84% and 84% respectively. The 9th and 10th modes are lateral modes at 322 Hz and they are very close to the 4th and 5th mode (transverse-tilting) of the gearbox at 324 Hz. Similarly, the 23rd and 24th modes of the global rotor system are the lateral mode at 710 Hz which is very close to the gearbox transverse-tilting mode at 711 Hz. These results show that some global torsional-axial and lateral modes are highly coupled with some of the rotational-axial and transverse-tilting modes of the planetary gearbox respectively.

The distribution of the total and the gearbox modal energy during a vibration cycle is shown in Figure 6 for the first nine modes. Not surprisingly, the total modal energy of the global rotor system is constant during the vibration period (transfer of energy from potential to kinetic and back, no losses in the undamped system) while the modal energy of the gearbox is fluctuating except for the 1st mode, which is a rigid body torsional mode. This makes perfect sense since the modal analysis was carried out for the global rotor system, and the modal energy of the global rotor system should be constant. However, the planetary gearbox is a part of the global rotor system and the modal analysis of the system was not carried out using the mass and stiffness matrices of the gearbox. Therefore, the modal energy of the planetary gearbox fluctuates during the vibration cycle. To capture this fluctuation, the time domain approach is used. Then, the mean value of the modal energy of the planetary gearbox was computed for each global mode by averaging the fluctuating modal energy, using the Eq. (28).

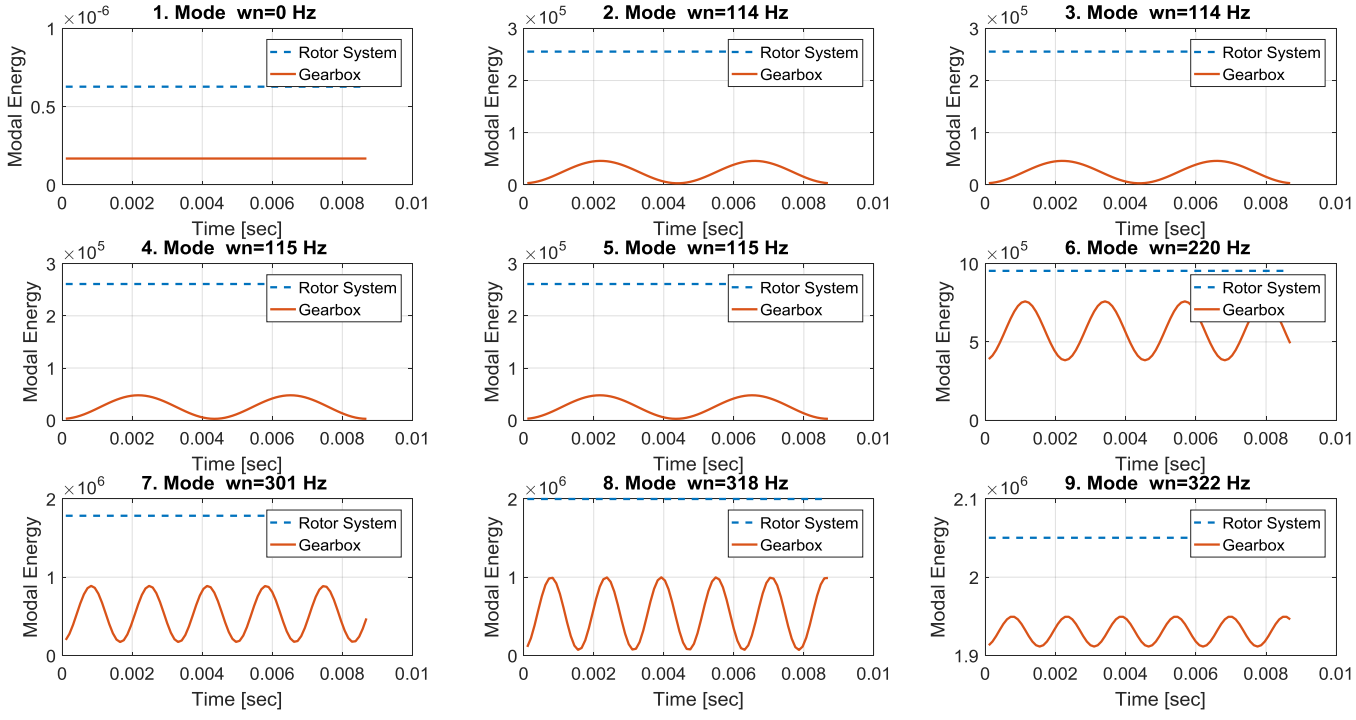

Figure 6: Modal energy of the helical planetary geared rotor system over time

3.2.2 Spur Planetary Geared Rotor

Modal analyses of the spur planetary geared rotor system and the planetary gearbox were carried out by setting the helix angle of all gears zero. The system and gearbox parameters from Table 1 and the assumptions from Section 3.2.1 were used for the analysis. The results in Table 3 show that modes of the shafts for the spur planetary geared rotor system are identified as torsional, axial, lateral and gearbox modes for the first thirty modes. Moreover, modes of the spur planetary gearbox are also identified as rotational, axial, translation, tilting and planet modes. The modes which are rotational-axial and translational-tilting in the helical planetary gearboxes become uncoupled in spur planetary gearboxes as rotational, axial, translational and tilting. Therefore, there is no coupling between the torsional, axial and lateral modes of the shafts.

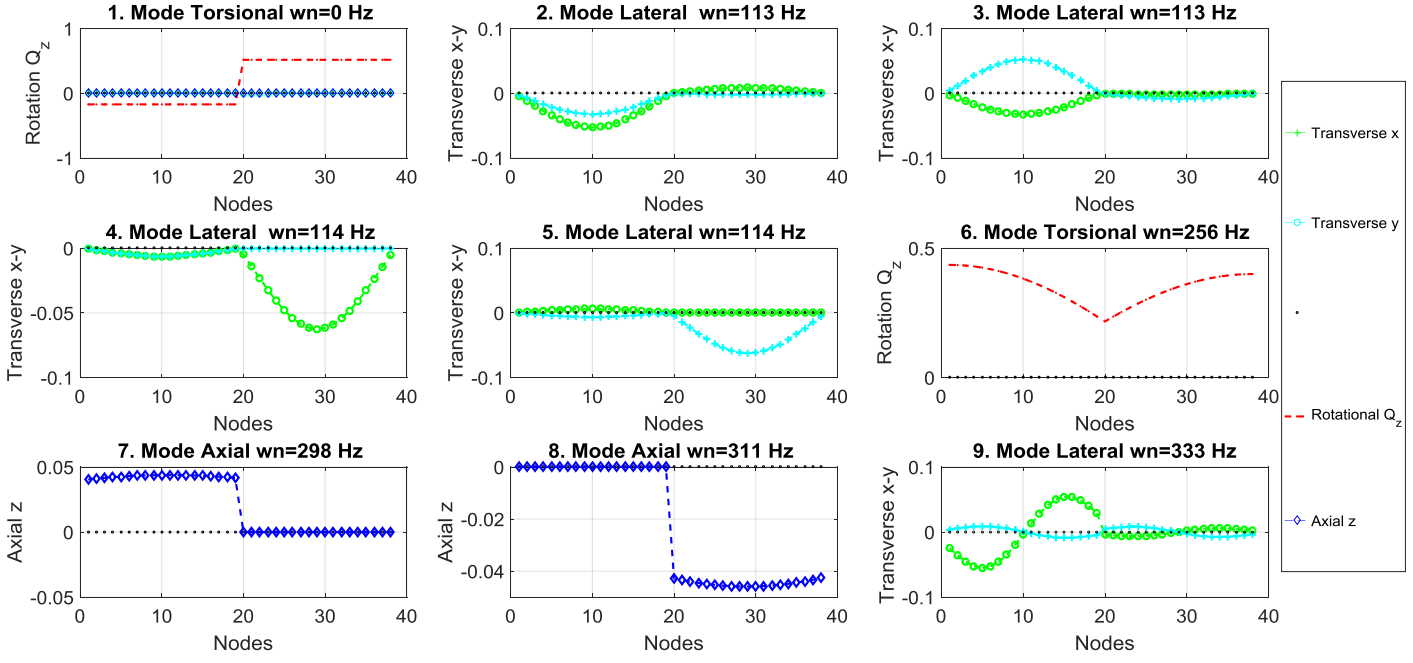

Figure 7: Mode shapes of the spur planetary geared rotor system

As seen in Figure 7, the first mode is once more the torsional rigid body mode. The other modes are torsional, axial and lateral modes. The 7th and 8th axial modes show that the input and output shafts have independent dynamic behaviour since there is

no deflection in the input shaft for the 7th axial mode and in the output shaft for the 8th mode. The reason for this phenomenon is that the axial component of the gear mesh stiffness is zero due to the zero-helix angle in the spur gear configuration. As a result, there cannot be vibration transmission between the output and input shafts in these independent axial modes. In other words, no axial response occurs in one shaft due to the axial excitation from the other shaft. The asymmetric motion described for the helical planetary geared rotor is also seen for the spur planetary geared rotor in Figure 7.

Table 3: Modes of the spur planetary geared rotor and just the gearbox

Spur Planetary Geared Rotor				Spur Planetary Gearbox	
Mode #	Gearbox Modal Energy %	Natural Frequency [Hz]	Mode Type	Natural Frequency [Hz]	Mode Type
1	27	0	Torsional (Rigid Body)	0	Rotational (Rigid Body)
2	10	113	Lateral	281	Tilting
3	10	113	Lateral	281	Tilting
4	8	114	Lateral	340	Tilting
5	8	114	Lateral	340	Tilting
6	57	256	Torsional	638	Axial
7	29	298	Axial	640	Translational
8	25	311	Axial	640	Translational
9	16	333	Lateral	666	Axial
10	16	333	Lateral	692	Rotational
11	100	340	Gearbox	738	Translational
12	100	340	Gearbox	738	Translational
13	10	345	Lateral	1077	Planet
14	10	345	Lateral	1081	Translational
15	21	473	Torsional	1081	Translational
16	62	509	Lateral	1462	Rotational
17	62	509	Lateral	1790	Axial
18	24	601	Lateral	1971	Translational
19	24	601	Lateral	1971	Translational
20	100	638	Gearbox	2197	Tilting
21	24	655	Lateral	2197	Tilting
22	24	655	Lateral	2332	Planet
23	89	727	Lateral	2376	Planet
24	89	727	Lateral	2385	Rotational
25	17	789	Torsional	2461	Translational
26	28	880	Lateral	2461	Translational
27	28	880	Lateral	2524	Planet
28	13	948	Lateral	2550	Rotational
29	13	948	Lateral	2835	Axial
30	100	1077	Gearbox	2898	Tilting

In some modes, modal energies of the planetary gearbox were also computed as 100%, which are the 11th, 12th, 20th, 30th gearbox modes respectively. These modes are associated with the 4th, 5th, 6th and 13th modes of the planetary gearbox and they were observed at exactly the same frequency for the global modes. Among these modes, the 4th, 5th and 6th modes are identified as carrier-planet, which means the carrier and planets can move freely and the 13th mode is identified as a planet mode, meaning that only the planets can move freely. Since the ring and sun gears do not move for these modes, no rotation or displacement occurs on the shafts. As a result, these modes are isolated from the shafts. The gearbox modal energies in Table 3 further highlight that even in the spur gear case some significant modal energy can be stored in the gearbox for some of the modes, highlighting the importance of the gearbox for the overall dynamic behaviour of the rotor system.

3.3. High Speed Modal Behaviour of the Helical Planetary Geared Rotor

Planetary geared rotors can work at higher operating speeds, and therefore gyroscopic moments can significantly affect their dynamic behaviour. To investigate the high speed dynamic behaviour of the helical planetary geared rotor system, modal analysis was carried out at 8000 rpm input speed and mode shapes are plotted for the first twelve modes in Figure 8. The speed ratio between the two shafts was determined as 3.04 based on the gear geometry given in Table 1. As a result, the input shaft rotates faster than the output shaft in this rotating system.

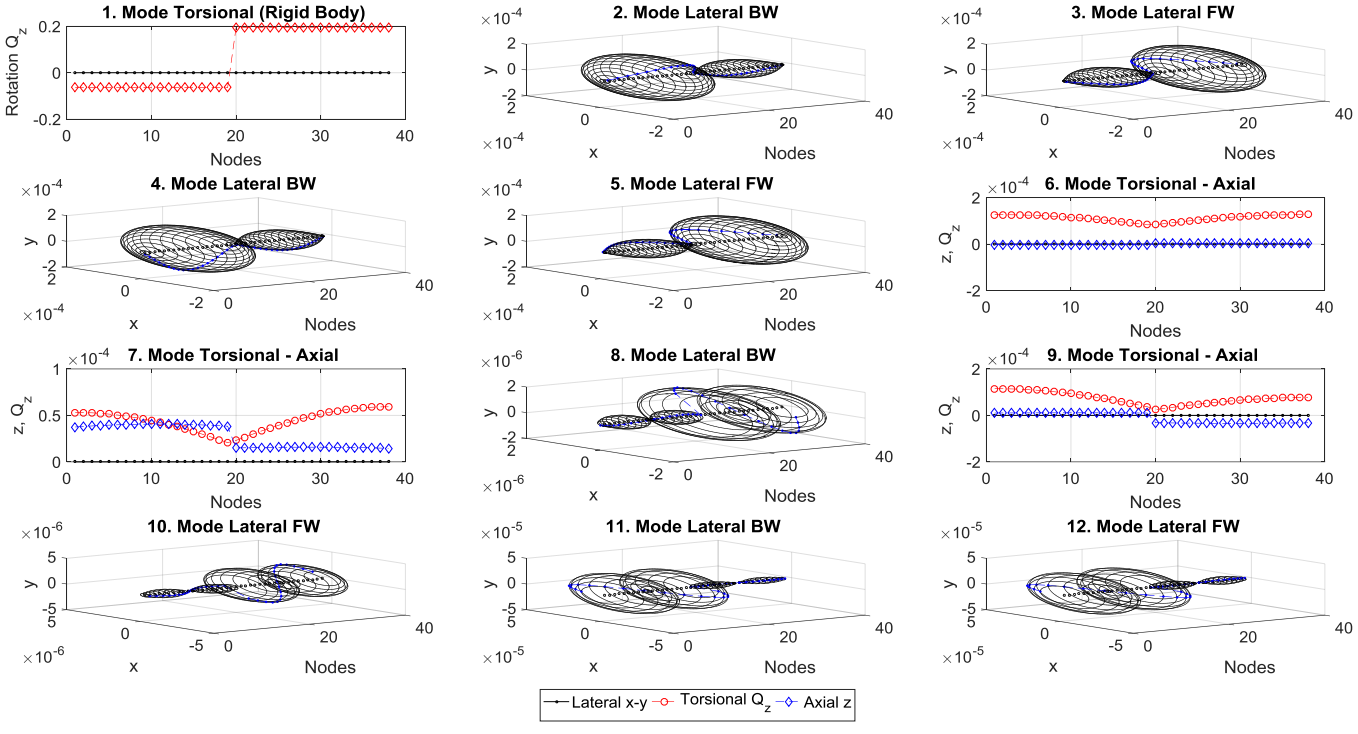

Figure 8: Mode shapes of the helical planetary geared rotor system at 8000 rpm

In contrast to the previous investigation, which focused on a static case, the orthogonal modes now combine to give lateral backward (BW) and forward (FW) whirling modes, while the coupled torsional-axial and torsional rigid body modes remain the same. The natural frequencies of the lateral backward and forward whirling modes are dependent on the shaft speeds due to the gyroscopic effect. On the other hand, there is no gyroscopic term in the axial and torsional components of the gyroscopic matrix, which leads to speed independent coupled torsional-axial modes.

Table 4: Low and high speed dynamic behaviour of the planetary geared rotor system

	100 rpm			8000 rpm		
Mode #	Natural Frequency [Hz]	Mode Type	Frequency Shift %	Natural Frequency [Hz]	Mode Type	Frequency Shift %
1	0.0	Torsional	0.000	0.0	Torsional	0.000
2	113.8	Lateral BW	0.001	113.4	Lateral BW	0.281
3	113.8	Lateral FW	0.000	113.5	Lateral FW	0.222
4	115.0	Lateral BW	0.001	115.2	Lateral BW	0.182
5	115.0	Lateral FW	0.001	115.3	Lateral FW	0.292
6	219.8	Torsional - Axial	0.000	219.8	Torsional - Axial	0.000
7	300.7	Torsional - Axial	0.000	300.7	Torsional - Axial	0.000
8	318.2	Torsional - Axial	0.000	317.8	Lateral BW	1.406
9	322.2	Lateral BW	0.017	318.2	Torsional - Axial	0.000
10	322.3	Lateral FW	0.017	326.6	Lateral FW	1.327
11	332.6	Lateral BW	0.003	331.8	Lateral BW	0.244
12	332.6	Lateral FW	0.003	333.3	Lateral FW	0.210

The speed dependent property of the lateral modes leads to a frequency split in the Campbell diagrams in Figure 9 where the natural frequencies of the lateral modes change with respect to the shaft speed whilst the torsional-axial modes are not affected by the shaft speeds. The forward whirling mode thereby experiences an increase in frequency, while the backward whirling mode sees a decrease in frequency.

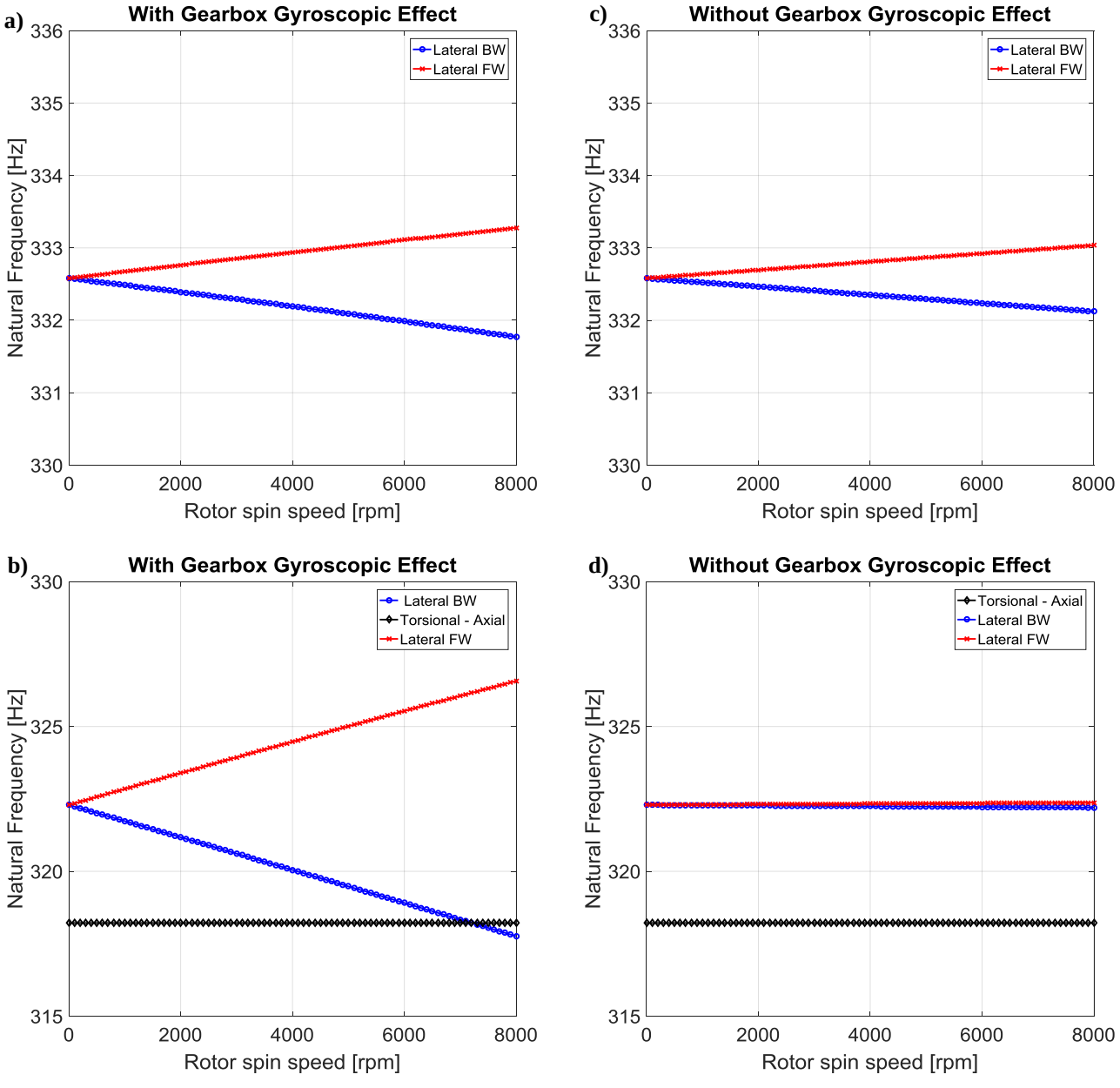

Figure 9: Campbell diagram, a) and b) with gearbox gyroscopic effect, c) and d) without gearbox gyroscopic effect for two different frequency ranges.

Gyroscopic moments can originate from the shafts and the rigid disk elements inside the planetary gearbox (gears and carrier). To understand the impact of the gearbox gyroscopic moments on the frequency response, Campbell diagrams were generated with and without gearbox gyroscopic effects for two frequency ranges in Figure 9. For instance, a significant gearbox gyroscopic effect is seen for the 9th and 10th lateral BW and FW modes (numbering from the static case). When plotting the Campbell diagram without the gearbox gyroscopic effect, the natural frequency change becomes very small for these modes. A small frequency change can still be observed due to the gyroscopic effects from the shafts. The frequency shifts between the static case and 8000 rpm for these modes are 1.41% and 1.33% respectively, as seen in Table 4. On the other hand, the gearbox gyroscopic effect is just visible for the 2nd, 3rd, 4th, 5th, 11th, 12th lateral modes. The frequency shifts between the static case and 8000 rpm are 0.28%, 0.22%, 0.18%, 0.29%, 0.24%, 0.21% for these modes, as seen in Table 4. The highest gearbox gyroscopic effect within the first twelve modes is observed for the 9th and 10th mode (in the static case) and the gearbox has a higher modal energy of about 94% for these modes. However, the gearbox has a lower modal energy at a value of 10% for the 2nd, 3rd, 4th

and 5th modes and 17% for the 11th and 12th modes. It can be concluded that the planetary gearbox gyroscopic effect is much more dominant in some modes where the planetary gearbox has higher modal energy.

Table 4 also provides data for a low speed (100 rpm) modal analysis, where the natural frequencies, mode types and frequency shifts can be compared to the high speed case (8000 rpm). It is clear that there is a natural frequency shift between the low and high speeds. To better understand the impact of the gyroscopic effects on the mode shapes, the Modal Assurance Criteria (MAC) is used to compare the eigenvectors at low and high speeds. The MAC formula is [65]

$$MAC(L,H) = \frac{\left|\{\phi_L\}_r^T\{\phi_H\}_q\right|^2}{\left(\{\phi_L\}_r^T\{\phi_L\}_r\right)\left(\{\phi_H\}_q^T\{\phi_H\}_q\right)} \tag{30}$$

where ϕ_L and ϕ_H are the low and high speed eigenvectors respectively, and r and q represent the corresponding mode number. The resulting MAC matrices with and without gyroscopic effects in the gearbox are shown in Figures 10a and b respectively.

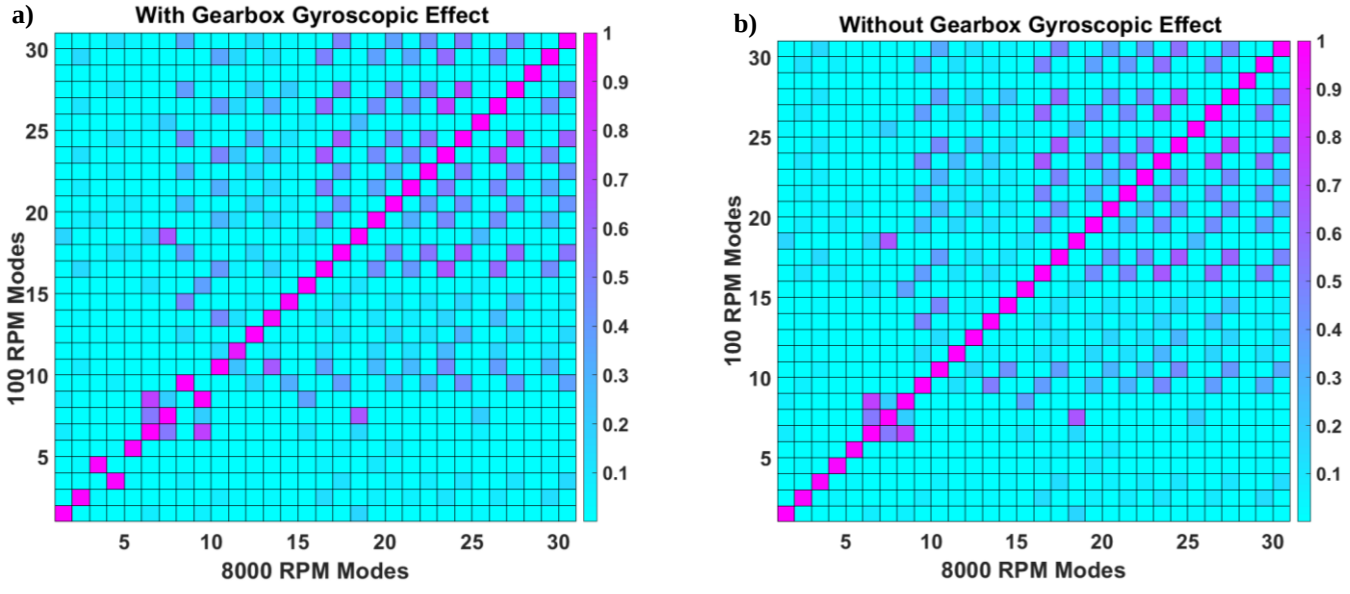

Figure 10: MAC matrices for low (100 rpm) and high (8000 rpm) speeds, a) with planetary gearbox gyroscopic effect, b) without planetary gearbox gyroscopic effect

The MAC matrix in Figure 10a shows that modes eight and nine reverse their order due to the crossing in Campbell diagram (veering), while the other modes do not seem to be affected by the shaft speed. A further reduction in speed dependence can be observed when the gyroscopic effects of the gearbox are neglected, leading to a nearly 100% MAC diagonal in Figure 10b. The MAC is not 100% in Figure 10b because there is a small gyroscopic effect from the two shafts. In summary, it can be said that the rotor dynamic behaviour is only mildly affected by the rotational speed, and for modes with a high gearbox contribution stronger splitting of the frequencies may lead to unexpected mode veering regions.

4. DISCUSSION

The main focus of this investigation is to understand the impact of an equally spaced planetary gearbox on the global dynamic behaviour of a planetary geared rotor system. Mode shapes of the helical planetary geared rotors are identified as coupled torsional-axial, lateral and gearbox modes whereas mode shapes with the spur gearbox become torsional, axial, lateral and gearbox. The main difference between the spur and helical planetary geared rotors is the presence of coupling between torsional and axial modes in the latter due to the helix angle. The helix angle effect can be clearly seen in the composition of the global stiffness matrix of the planetary geared rotors in Figure 11. Here, it is clear that zero helix angle makes the gear mesh stiffness zero in the axial directions. Therefore, the input and output shafts have independent dynamic behaviours from each other in the axial modes, and the axial vibrations cannot transmit between them. Moreover, making the helix angle zero cancels the coupling term between the axial and torsional directions, resulting in uncoupled torsional, axial and lateral modes. In the case of helical gears, axial thrust forces can create unexpected torsional excitations on the shaft, which can be of great significance for geared turbofan engines where planetary gearboxes are commonly used [56].

A further feature of the modes for both spur and helical planetary geared rotors is the asymmetric motion in the two shafts, although the planetary gearbox is located at the middle of the system and the shafts have identical properties. This breaking of

the symmetry can be attributed to the different mass and inertia properties of the input and output members of the planetary gearbox itself, which are directly attached to the two shafts.

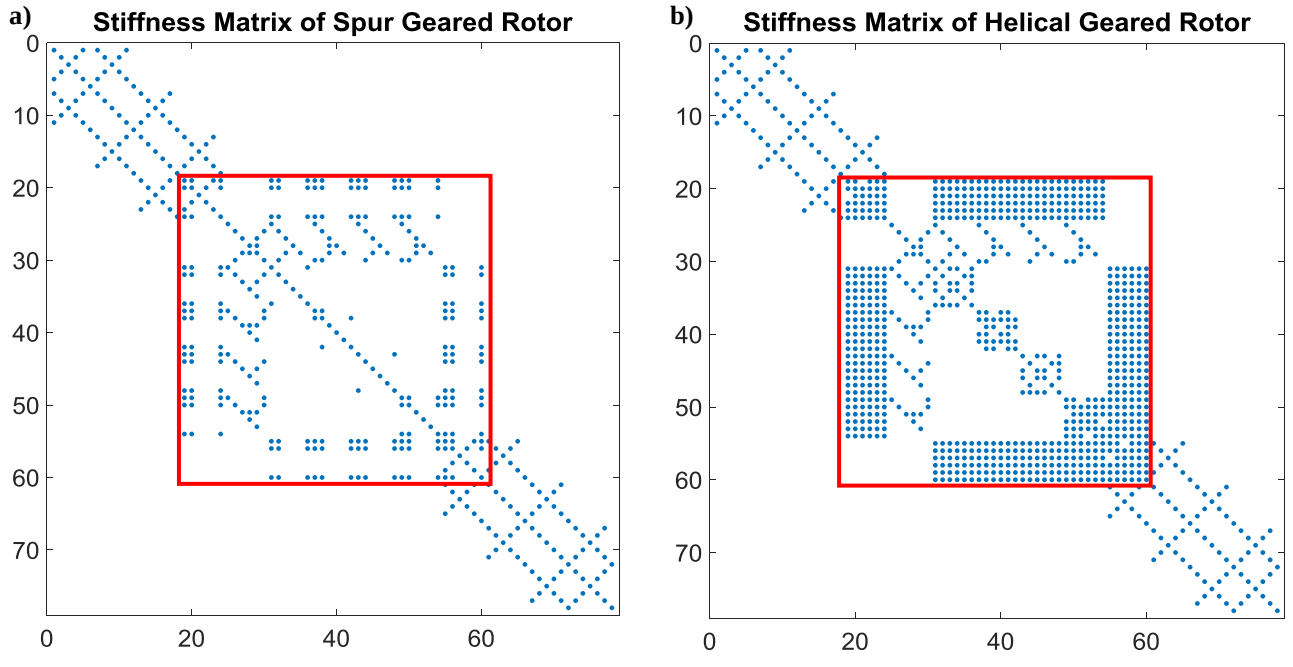

Figure 11: Helix angle effect on the global stiffness matrix, a) spur, b) helical

To better understand the contribution of the gearbox to the global modes of the system, the modal energy of the gearbox compared to the total modal energy of the system has been computed. Table 2 and 3 summarise the results of this analysis for a) the helical and b) the spur gear configuration. It shows that there are some global modes in which no motion of the shaft is observed and all the energy is stored in the gearbox. These modes can be directly related to the internal modes of the planetary gearbox where the planets or planets and carrier move in the case of the helical or spur planetary gearbox respectively, while the central members do not move, leading to a decoupling of the gearbox and the shafts. They are classified as gearbox modes in the global rotor system. In contrast to these internal gearbox modes, the other modes in which the planetary gearbox has higher modal energy are highly coupled with the shafts. For these modes, the natural frequencies of the rotor system and planetary gearbox are very close to each other.

An additional effect that needs to be considered when studying the dynamics of a geared rotor system is the gyroscopic effect originating from the planetary gearbox. This can lead to a mode veering phenomenon in the MAC comparison between low (100 rpm) and high (8000 rpm) speeds. In addition, they can significantly influence the natural frequencies of the backward and forward lateral modes of the geared rotor system, particularly for the modes with higher gearbox modal energy.

5. CONCLUSION

The dynamic behaviours of two shaft rotor systems with equally spaced spur and helical planetary gearboxes were investigated in detail by considering the gyroscopic effects and neglecting damping. For this purpose, a six degrees of freedom dynamic model was presented, combining a lumped parameter model of the planetary gearbox with Timoshenko beam elements for the shafts. Members of the planetary gearbox, which are the ring, planet and sun gears and carrier, were assumed to be rigid disks and the gear contacts were considered as flexible. The generated model was used to conduct a modal analysis of the global response of the geared rotor system to study the impact of the planetary gearbox on the modal behaviour of the shafts. On the basis of mode shapes of the shafts, mode identification of the rotor system was carried out for the static case and the rotating case (including gyroscopic effects). The effect of the planetary gearbox on each global rotor mode was then quantified for the static case by a modal energy analysis. The effect of the planetary gearbox gyroscopic terms on the global rotor modes was also investigated.

The modal analysis of the planetary geared rotor system highlighted the strong modal coupling introduced by the gearbox. Modes of the helical planetary geared rotors are identified as coupled torsional-axial, lateral and gearbox modes whereas spur planetary geared rotors have uncoupled modes, which are classified as axial, torsional, lateral modes and gearbox modes. The gear helix angle is the main coupling parameter in planetary geared rotor systems, which makes torsional and axial modes

coupled. It is also found that axial vibrations of the input and output shafts are uncoupled from each other in spur planetary geared rotors. In helical planetary geared rotors, coupled torsional-axial modes can also result in mode shape decoupling in the axial direction between the input and output shafts of the planetary gearbox due to the lower axial stiffness of the planetary gearbox compared to the shaft stiffness. Gearbox modes are fully isolated from the shafts because no dynamic interaction between the shafts and gearbox occurs for these modes. Also, no displacement and rotation occur on the shafts for the gearbox modes. Therefore, the modal energy of the planetary gearbox for the gearbox modes is 100%. The natural frequencies of the gearbox modes, computed with a global rotor modal analysis, are directly associated with the planet modes, computed with an independent modal analysis of the planetary gearbox. Apart from the gearbox modes, the planetary gearbox has higher modal energy in some other modes where the coupling level between the gearbox and shafts is much higher. At these modes, natural frequencies of the planetary geared rotor system and the planetary gearbox are close to each other. This clearly shows that gearbox is dominant when there is a highly coupling between the global rotor system and gearbox. As a result of the dominancy of the gearbox, the natural frequencies computed from the independent modal analysis of the gearbox and the global rotor system become closer to each other. For the high speed dynamic behaviour, the global backward and forward lateral modes in which the planetary gearbox has higher modal energy can experience significant gyroscopic effects due to the gearbox members. This can lead to significant changes in natural frequencies of the global system. When compared to the gyroscopic effects originating from the shafts, the gyroscopic effects of the planetary gearbox can result in a mode veering phenomenon.

It can be concluded that for an accurate dynamic response prediction of a planetary geared rotor system, it is absolutely necessary to incorporate a reasonably detailed planetary gearbox model in the system in order to capture the detected complicated mode coupling events and the frequency shifting and mode veering phenomena at higher speeds. Not including these effects will lead to significantly less accurate results.

ACKNOWLEDGMENT

This study was funded by the Ministry of National Education of the Republic of Turkey. The authors thank Prof. Dr. Kenan Yüce Şanlıtürk and Dr. Tugan Eritenel for their useful suggestions and comments.

NOMENCLATURE

q	Generalized coordinates
ξ	Natural coordinates
d	Diameter of shaft
l_e	Length of a beam element
ρ_e	Material density of beam elements
A_e	Cross section area of beam elements
I_e	Second moment of area of beam elements
J_e	Polar moment of area of beam elements
E_e	Elasticity modulus of beam elements
G_e	Shear modulus of beam elements
ν_e	Poisson`s ratio
α_1, α_2	Proportional damping constants
N	Number of planets
r_c	Radius of carrier
m	Mass
I_d	Diametral mass moment of inertia
I_p	Polar mass moment of inertia
$\boldsymbol{\Omega}$	Rotating speed of elements
k_x	Support bearing stiffness in x direction
k_y	Support bearing stiffness in y direction
k_z	Support bearing stiffness in z direction
k_{Q_x}	Support bearing stiffness in Q_x direction
k_{Q_y}	Support bearing stiffness in Q_y direction
k_{Q_z}	Support bearing stiffness in Q_z direction
c_x	Support bearing damping in x direction
c_y	Support bearing damping in y direction
c_z	Support bearing damping in z direction
c_{Q_x}	Support bearing damping in Q_x direction
c_{Q_y}	Support bearing damping in Q_y direction
c_{Q_z}	Support bearing damping in Q_z direction
T	Kinetic energy
V	Potential energy
L	Total energy
ε	Modal energy ratio
rpm	Revolution per minute
DOF	Degree of freedom
Subscripts	
$h = r, c, s$	Central member index
r	Ring gear
c	Carrier
s	Sun gear
p	Planet gear

REFERENCES

[1] J. Yang, L. Dai, Survey of dynamics of planetary gear trains, International Journal of Materials and Structural Integrity. 1 (2008) 302–322.

[2] C.G. Cooley, R.G. Parker, A review of planetary and epicyclic gear dynamics and vibrations research, Applied Mechanics Reviews. 66 (2014) 40804.

[3] A. Kahraman, R. Singh, Non-linear dynamics of a spur gear pair, Journal of Sound and Vibration. 142 (1990) 49–75.

[4] H. Nevzat Özgüven, D.R. Houser, Mathematical models used in gear dynamics—A review, Journal of Sound and Vibration. 121 (1988) 383–411. doi:10.1016/S0022-460X(88)80365-1.

[5] A. Kahraman, Planetary Gear Train Dynamics, Journal of Mechanical Design. 116 (1994) 713. doi:10.1115/1.2919441.

[6] J. Lin, R.G. Parker, Analytical Characterization of the Unique Properties of Planetary Gear Free Vibration, Journal of Vibration and Acoustics. 121 (1999) 316–321. doi:10.1115/1.2893982.

[7] T. Eritenel, R.G. Parker, Modal properties of three-dimensional helical planetary gears, Journal of Sound and Vibration. 325 (2009) 397–420. doi:10.1016/j.jsv.2009.03.002.

[8] C.G. Cooley, R.G. Parker, Vibration Properties of High-Speed Planetary Gears With Gyroscopic Effects, Journal of Vibration and Acoustics. 134 (2012) 061014. doi:10.1115/1.4006646.

[9] L. Zhang, Y. Wang, K. Wu, R. Sheng, Q. Huang, Dynamic modeling and vibration characteristics of a two-stage closed-form planetary gear train, Mechanism and Machine Theory. 97 (2016) 12–28. doi:10.1016/j.mechmachtheory.2015.10.006.

[10] L. Zhang, Y. Wang, K. Wu, R. Sheng, Three-Dimensional Modeling and Structured Vibration Modes of Two-Stage Helical Planetary Gears Used in Cranes, Shock and Vibration. 2017 (2017) 10–19. doi:10.1155/2017/9864959.

[11] M. Inalpolat, A. Kahraman, Dynamic modelling of planetary gears of automatic transmissions, Proceedings of the Institution of Mechanical Engineers, Part K: Journal of Multi-Body Dynamics. 222 (2008) 229–242. doi:10.1243/14644193JMBD138.

[12] W. Sun, X. Ding, J. Wei, X. Hu, Q. Wang, An analyzing method of coupled modes in multi-stage planetary gear system, International Journal of Precision Engineering and Manufacturing. 15 (2014) 2357–2366. doi:10.1007/s12541-014-0601-9.

[13] J. Wang, Y. Wang, Z. Huo, Analysis of dynamic behavior of multiple-stage planetary gear train used in wind driven generator, The Scientific World Journal. 2014 (2014). doi:10.1155/2014/627045.

[14] H. Zhai, C. Zhu, C. Song, H. Liu, G. Li, F. Ma, Dynamic modeling and analysis for transmission system of high-power wind turbine gearbox, Journal of Mechanical Science and Technology. 29 (2015) 4073–4082. doi:10.1007/s12206-015-0901-8.

[15] J. Wei, A. Zhang, D. Qin, T.C. Lim, R. Shu, X. Lin, F. Meng, A coupling dynamics analysis method for a multistage planetary gear system, Mechanism and Machine Theory. 110 (2017) 27–49. doi:10.1016/j.mechmachtheory.2016.12.007.

[16] A. Zhang, J. Wei, D. Qin, S. Hou, Analytical coupling characterization of multi-stage planetary gear free vibration considering flexible structure, Journal of Vibroengineering. 19 (2017) 3994–4008. doi:10.21595/jve.2017.17767.

[17] A. Kahraman, Free torsional vibration characteristics of compound planetary gear sets, Mechanism and Machine Theory. 36 (2001) 953–971. doi:10.1016/S0094-114X(01)00033-7.

[18] S. Dhouib, R. Hbaieb, F. Chaari, M.S. Abbes, T. Fakhfakh, M. Haddar, Free vibration characteristics of compound planetary gear train sets, Proceedings of the Institution of Mechanical Engineers, Part C: Journal of Mechanical Engineering Science. 222 (2008) 1389–1401. doi:10.1243/09544062JMES870.

[19] D.R. Kiracofe, R.G. Parker, Structured Vibration Modes of General Compound Planetary Gear Systems, Journal of Vibration and Acoustics. 129 (2007) 1. doi:10.1115/1.2345680.

[20] Y. Guo, R.G. Parker, Purely rotational model and vibration modes of compound planetary gears, Mechanism and Machine Theory. 45 (2010) 365–377. doi:10.1016/j.mechmachtheory.2009.09.001.

[21] P. Sondkar, Dynamic modeling of double-helical planetary gear sets, The Ohio State University, 2012.

[22] P. Sondkar, A. Kahraman, A dynamic model of a double-helical planetary gear set, Mechanism and Machine Theory. 70 (2013) 157–174. doi:10.1016/j.mechmachtheory.2013.07.005.

[23] Z. Sheng, J. Tang, S. Chen, Z. Hu, Modal Analysis of Double-Helical Planetary Gears With Numerical and Analytical Approach, Journal of Dynamic Systems, Measurement, and Control. 137 (2015) 041012. doi:10.1115/1.4028788.

[24] S. Mo, Y. Zhang, Q. Wu, H. Houjoh, S. Matsumura, Research on natural characteristics of double-helical star gearing system for GTF aero-engine, Mechanism and Machine Theory. 106 (2016) 166–189. doi:10.1016/j.mechmachtheory.2016.09.001.

[25] M. K Khoozani, M. Poursina, A. P Anaraki, Study of gyroscopic effects on the dynamics and vibrations of double-helical planetary gear set, Proceedings of the Institution of Mechanical Engineers, Part K: Journal of Multi-Body Dynamics. 0 (2017) 1–25. doi:10.1177/1464419317725947.

[26] V. Abousleiman, P. Velex, A hybrid 3D finite element/lumped parameter model for quasi-static and dynamic analyses of planetary/epicyclic gear sets, Mechanism and Machine Theory. 41 (2006) 725–748. doi:10.1016/j.mechmachtheory.2005.09.005.

[27] V. Abousleiman, P. Velex, S. Becquerelle, Modeling of Spur and Helical Gear Planetary Drives With Flexible Ring Gears and Planet Carriers, Journal of Mechanical Design. 129 (2007) 95. doi:10.1115/1.2359468.

[28] X. Wu, R.G. Parker, Modal Properties of Planetary Gears With an Elastic Continuum Ring Gear, Journal of Applied Mechanics. 75 (2008) 031014. doi:10.1115/1.2839892.

[29] R.G. Parker, X. Wu, Vibration modes of planetary gears with unequally spaced planets and an elastic ring gear, Journal of Sound and Vibration. 329 (2010) 2265–2275. doi:10.1016/j.jsv.2009.12.023.

[30] Z. Chen, Y. Shao, D. Su, Dynamic simulation of planetary gear set with flexible spur ring gear, Journal of Sound and Vibration. 332 (2013) 7191–7204. doi:10.1016/j.jsv.2013.07.026.

[31] J.L.M. Peeters, D. Vandepitte, P. Sas, Analysis of internal drive train dynamics in a wind turbine, Wind Energy. 9 (2006) 141–161. doi:10.1002/we.173.

[32] M. Zhao, J. Ji, Dynamic analysis of wind turbine gearbox components, Energies. 9 (2016) 1–18. doi:10.3390/en9020110.

[33] D.C. Fyler, M. Inalpolat, A Dynamic Model for Double-Planet Planetary Gearsets, Journal of Vibration and Acoustics. 138 (2016) 021006. doi:10.1115/1.4032181.

[34] F. Concli, L. Cortese, R. Vidoni, F. Nalli, G. Carabin, A mixed FEM and lumped-parameter dynamic model for evaluating the modal properties of planetary gearboxes †, Journal of Mechanical Science and Technology. 32 (2018) 3047–3056. doi:10.1007/s12206-018-0607-9.

[35] J. Lin, R.G. Parker, Sensitivity of planetary gear natural frequencies and vibration modes to model parameters, Journal of Sound and Vibration. 228 (1999) 109–128.
[36] Y. Guo, R.G. Parker, Sensitivity of General Compound Planetary Gear Natural Frequencies and Vibration Modes to Model Parameters, Journal of Vibration and Acoustics. 132 (2010) 011006. doi:10.1115/1.4000461.
[37] T.M. Ericson, R.G. Parker, Planetary gear modal vibration experiments and correlation against lumped-parameter and finite element models, Journal of Sound and Vibration. 332 (2013) 2350–2375. doi:10.1016/j.jsv.2012.11.004.
[38] A. Hammami, A.F. Del Rincon, F.V. Rueda, F. Chaari, M. Haddar, Modal analysis of back-to-back planetary gear: experiments and correlation against lumped-parameter model, Journal of Theoretical and Applied Mechanics. (2015) 125. doi:10.15632/jtam-pl.53.1.125.
[39] A. Mbarek, A.F. Del Rincon, A. Hammami, M. Iglesias, F. Chaari, F. Viadero, M. Haddar, Comparison of experimental and operational modal analysis on a back to back planetary gear, Mechanism and Machine Theory. 124 (2018) 226–247. doi:10.1016/j.mechmachtheory.2018.03.005.
[40] J.W. David, L.D. Mitchell, Linear dynamic coupling in geared rotor systems, Journal of Vibration, Acoustics, Stress, and Reliability in Design. 108 (1986) 171–176.
[41] A. Kahraman, H. Ozguven, D.. Houser, Dynamic analysis of geared rotors by finite elements, Journal of Mechanical Design. 114 (1992) 507–514. doi:10.1115/1.2926579.
[42] J.S. Rao, T.N. Shiau, J.R. Chang, Theoretical Analysis of Lateral Response Due to Torsional Excitation of Geared Rotors, Mechanism and Machine Theory. (1998). doi:10.1016/S0094-114X(97)00056-6.
[43] T.N. Shiau, J.S. Rao, J.R. Chang, S.-T. Choi, Dynamic Behavior of Geared Rotors, Journal of Engineering for Gas Turbines and Power. 121 (1999) 494–503.
[44] Y. Zhang, Q. Wang, H. Ma, J. Huang, C. Zhao, Dynamic analysis of three-dimensional helical geared rotor system with geometric eccentricity, Journal of Mechanical Science and Technology. 27 (2013) 3231–3242. doi:10.1007/s12206-013-0846-8.
[45] S. Chen, J. Tang, C. Zhou, Z. Hu, Modal and whirling analysis of coupled lateral and torsional vibration of herringbone gear, International Journal of Dynamics and Control. 2 (2014) 404–414. doi:10.1007/s40435-013-0042-9.
[46] C.F. Li, S.H. Zhou, J. Liu, B.C. Wen, Coupled lateral-torsional-axial vibrations of a helical gear-rotor-bearing system, Acta Mechanica Sinica. 30 (2014) 746–761. doi:10.1007/s10409-014-0063-4.
[47] S. Zhou, Z. Ren, G. Song, B. Wen, Dynamic Characteristics Analysis of the Coupled Lateral-Torsional Vibration with Spur Gear System, International Journal of Rotating Machinery. 2015 (2015). doi:10.1155/2015/371408.
[48] S. Chen, J. Tang, Y. Li, Z. Hu, Rotordynamics analysis of a double-helical gear transmission system, Meccanica. 51 (2015) 251–268. doi:10.1007/s11012-015-0194-0.
[49] Z. Hu, J. Tang, S. Chen, Analysis of coupled lateral-torsional vibration response of a geared shaft rotor system with and without gyroscopic effect, Journal of Mechanical Engineering Science. (2018) 1–14. doi:10.1177/0954406217753457.
[50] W. Shi, C.-W. Kim, C.-W. Chung, H.-C. Park, Dynamic Modeling and Analysis of a Wind Turbine Drivetrain Using the Torsional Dynamic Model, International Journal of Precision Engineering And Manufacturing. 14 (2013) 153–159. doi:10.1007/s12541-013-0021-2.
[51] H.-L. Yao, Y. Liu, Z.-H. Ren, B.-C. Wen, C.-F. Li, Research on Dynamic Modeling and Analysis of the Coupled Planetary Gear and Rotor System, in: P. Pennacchi (Ed.), Proceedings of the 9th IFToMM International Conference on Rotor Dynamics, Springer International Publishing, Cham, 2015: pp. 1323–1331. doi:10.1007/978-3-319-06590-8_108.
[52] S. Wei, J. Zhao, Q. Han, F. Chu, Dynamic response analysis on torsional vibrations of wind turbine geared transmission system with uncertainty, Renewable Energy. 78 (2015) 60–67. doi:10.1016/j.renene.2014.12.062.
[53] C. Zhu, S. Chen, C. Song, H. Liu, H. Bai, F. Ma, Dynamic analysis of a megawatt wind turbine drive train, Journal of Mechanical Science and Technology. 29 (2015) 1913–1919. doi:10.1007/s12206-015-0413-6.
[54] J. Helsen, F. Vanhollebeke, B. Marrant, D. Vandepitte, W. Desmet, Multibody modelling of varying complexity for modal behaviour analysis of wind turbine gearboxes, Renewable Energy. 36 (2011) 3098–3113. doi:10.1016/j.renene.2011.03.023.
[55] X. Jin, L. Li, W. Ju, Z. Zhang, X. Yang, Multibody modeling of varying complexity for dynamic analysis of large-scale wind turbines, Renewable Energy. 90 (2016) 336–351. doi:10.1016/j.renene.2016.01.003.
[56] A. Tatar, C.W. Schwingshackl, Effect of a Planetary Gearbox on the Dynamics of a Rotor System, in: ASME Turbo Expo 2018: Turbomachinery Technical Conference and Exposition, American Society of Mechanical Engineers, Oslo, 2018: pp. 1–11.
[57] J. Wei, P. Bai, D. Qin, T.C. Lim, P. Yang, H. Zhang, Study on vibration characteristics of fan shaft of geared turbofan engine with sudden imbalance caused by blade off, Journal of Vibration and Acoustics. 140 (2018) 41010.
[58] M.I. Friswell, Dynamics of rotating machines, Cambridge University Press, 2010.
[59] J.S. Rao, History of rotating machinery dynamics, Springer Science & Business Media, 2011.
[60] S. Adhikari, Damping models for structural vibration, (2001).
[61] P. Lynwander, Gear drive systems: Design and application, CRC Press, 1983.
[62] A. Tatar, L. Salles, A.H. Haslam, C.W. Schwingshackl, Comparison of Computational Generalized and Standard Eigenvalue Solutions of Rotating Systems, in: M. Mains, B.J. Dilworth (Eds.), Topics in Modal Analysis & Testing, Volume 9, Springer International Publishing, 2018. doi:10.1007/978-3-319-74700-2.
[63] D.J. Inman, Engineering vibration, Prentice Hall New Jersey, 2008.
[64] H. Koruk, K.Y. Sanliturk, A novel definition for quantification of mode shape complexity, Journal of Sound and Vibration. 332 (2013) 3390–3403. doi:10.1016/j.jsv.2013.01.039.
[65] D.J. Ewins, Modal testing: theory, practice, and application, Research Studies Press, 2000.